

# CH<sub>3</sub>OCH<sub>3</sub> in Orion-KL: a striking similarity with HCOOCH<sub>3</sub><sup>★</sup>

N. Brouillet<sup>1,2</sup>, D. Despois<sup>1,2</sup>, A. Baudry<sup>1,2</sup>, T.-C. Peng<sup>1,2</sup>, C. Favre<sup>3</sup>, A. Wootten<sup>4</sup>, A. J. Remijan<sup>4</sup>, T. L. Wilson<sup>5</sup>, F. Combes<sup>6</sup>, and G. Wlodarczak<sup>7</sup>

<sup>1</sup> Univ. Bordeaux, LAB, UMR 5804, F-33270 Floirac, France

e-mail: brouillet, despois, baudry@obs.u-bordeaux1.fr

<sup>2</sup> CNRS, LAB, UMR 5804, F-33270 Floirac, France

<sup>3</sup> Department of Physics and Astronomy, University of Århus, Ny Munkegade 120, DK-8000 Århus C, Denmark

e-mail: favre@phys.au.dk

<sup>4</sup> National Radio Astronomy Observatory, 520 Edgemont Road, Charlottesville, VA 22903-2475, USA

e-mail: awootten, aremijan@nrao.edu

<sup>5</sup> Naval Research Laboratory, Code 7210, Washington, DC 20375, USA

e-mail: tom.wilson@nrl.navy.mil

<sup>6</sup> Observatoire de Paris, LERMA, CNRS, 61 Av. de l'Observatoire, 75014 Paris, France

e-mail: francoise.combes@obspm.fr

<sup>7</sup> Laboratoire de Physique des Lasers, Atomes et Molécules, Université de Lille1, UMR 8523, 59655 Villeneuve d'Ascq Cedex, France

e-mail: georges.wlodarczak@univ-lille1.fr

Received 11 July 2012; accepted 05 December 2012

## ABSTRACT

**Context.** Orion-KL is a remarkable, nearby star-forming region where a recent explosive event has generated shocks that could have released complex molecules from the grain mantles.

**Aims.** A comparison of the distribution of the different complex molecules will help in understanding their formation and constraining the chemical models.

**Methods.** We used several data sets from the Plateau de Bure Interferometer to map the dimethyl ether emission with different arcsec spatial resolutions and different energy levels (from  $E_{\text{up}}=18$  to 330 K) to compare with our previous methyl formate maps.

**Results.** Our data show remarkable similarity between the dimethyl ether (CH<sub>3</sub>OCH<sub>3</sub>) and the methyl formate (HCOOCH<sub>3</sub>) distributions even on a small scale (1.8''×0.8'' or ~ 500 AU). This long suspected similarity, seen from both observational and theoretical arguments, is demonstrated with unprecedented confidence, with a correlation coefficient of maps ~ 0.8.

**Conclusions.** A common precursor is the simplest explanation of our correlation. Comparisons with previous laboratory work and chemical models suggest the major role of grain surface chemistry and a recent release, probably with little processing, of mantle molecules by shocks. In this case the CH<sub>3</sub>O radical produced from methanol ice would be the common precursor (whereas ethanol, C<sub>2</sub>H<sub>5</sub>OH, is produced from the radical CH<sub>2</sub>OH). The alternative gas phase scheme, where protonated methanol CH<sub>3</sub>OH<sub>2</sub><sup>+</sup> is the common precursor to produce methyl formate and dimethyl ether through reactions with HCOOH and CH<sub>3</sub>OH, is also compatible with our data. Our observations cannot yet definitely allow a choice between the different chemical processes, but the tight correlation between the distributions of HCOOCH<sub>3</sub> and CH<sub>3</sub>OCH<sub>3</sub> strongly contrasts with the different behavior we observe for the distributions of ethanol and formic acid. This provides a very significant constraint on models.

**Key words.** Astrochemistry – ISM: molecules – Radio lines: ISM – ISM: individual objects: Orion-KL

## 1. Introduction

The Orion protocluster region is the closest high mass star formation region to the Sun. We adopt a distance of 414±7 pc (Menten et al. 2007), consistent within the error bars with the values of 389 pc of Sandstrom et al. (2007), 437 pc of Hirota et al. (2007) and 419 pc of Kim et al. (2008). This region is remarkable because of the presence of high speed shocks which appear to be generated in the center of the Kleiman-Low infrared nebula Orion-KL. These are reminiscent of a past explosive event and are most clearly seen in the H<sub>2</sub> 2.12 μm emission (Allen & Burton 1993). From VLA proper motion measurements of two strong centimetric radiosources, it was proposed

that a very unique phenomenon had taken place some 500-1000 years ago: the close encounter, or collision, of two or more rather massive stars. The objects involved in such a dynamical interaction could have included the Becklin-Neugebauer object (BN) and sources I and n (Gómez et al. 2005; Rodríguez et al. 2005; Goddi et al. 2011; Nissen et al. 2012). Traces of this explosive pattern have recently been observed in the CO distribution by Zapata et al. (2009).

This very recent and energetic event at the heart of the nebula provides unique conditions for the study of a rich interstellar chemistry. Many molecules could have been released from the grain mantles because of dust heating or sputtering by multiple shocks, especially the relatively large molecules for which no gas-phase-only formation route is satisfactory.

From a set of twelve Plateau de Bure observations, we have recently analyzed the deuterated methanol isotopologues

<sup>★</sup> Based on observations carried out with the IRAM Plateau de Bure Interferometer. IRAM is supported by INSU/CNRS (France), MPG (Germany) and IGN (Spain).

**Table 1.** Main parameters of the IRAM Plateau de Bure interferometer data sets where transitions of dimethyl ether are detected.

Bandwidth (GHz)	HPBW ( $''$ )	Spectral resolution (MHz)	( $\text{km s}^{-1}$ )	Flux conversion ( $1 \text{ Jy beam}^{-1}$ )	Synthesized beam ( $'' \times ''$ )	PA ( $^\circ$ )	Pixel size ( $'' \times ''$ )
80.502 - 80.574 <sup>a</sup>	60	0.625	2.33	4.6 K	$7.63 \times 5.35$	15	$0.80 \times 0.80$
101.178 - 101.717 <sup>b</sup>	50	0.625	1.85	15.8 K	$3.79 \times 1.99$	22	$0.50 \times 0.50$
203.411 - 203.483 <sup>a</sup>	25	0.625	0.92	7.0 K	$2.94 \times 1.44$	27	$0.32 \times 0.32$
223.408 - 223.941 <sup>b</sup>	23	0.625	0.84	17.3 K	$1.79 \times 0.79$	14	$0.25 \times 0.25$

<sup>a</sup> Observations centered on ( $\alpha_{J2000} = 05^h35^m14^s.46$ ,  $\delta_{J2000} = -05^\circ22'30''.59$ ) with a velocity of 6  $\text{km s}^{-1}$  with respect to the LSR.

<sup>b</sup> Observations centered on ( $\alpha_{J2000} = 05^h35^m14^s.20$ ,  $\delta_{J2000} = -05^\circ22'36''.00$ ) with a velocity of 8  $\text{km s}^{-1}$  with respect to the LSR.

CH<sub>2</sub>DOH and CH<sub>3</sub>OD (Peng et al. 2012) and the methyl formate HCOOCH<sub>3</sub> (Favre et al. 2011a) emission in Orion KL. The latter work suggests a rather close morphological relation in several places of the Orion KL nebula between excited H<sub>2</sub> emission at 2.12  $\mu\text{m}$  and methyl formate.

Even though both methyl formate and dimethyl ether are oxygen-bearing molecules of medium complexity and both can be produced from gaseous methanol (e.g. Peeters et al. 2006) and/or from grain surface chemistry (e.g. Garrod et al. 2008), these two species are spectroscopically different, and their spectra behave differently with physical temperature. Furthermore, since the early days of dimethyl ether studies (Snyder et al. 1974; Clark et al. 1979) there was a hint of limited departures from LTE for dimethyl ether. Recently, we have carried out observations at the EVLA of the  $J(K_{-1}, K_{+1}) = 6(1,5) - 6(0,6)$  EE transition of dimethyl ether at 43.4475415 GHz (Favre et al. 2011b) which shows that the distribution is very similar to that of methyl formate.

In this paper we present the analysis of several dimethyl ether lines present in our Plateau de Bure data set. The maps of the CH<sub>3</sub>OCH<sub>3</sub> emission at different frequencies and energy levels are shown in Sect. 3. In Sect. 4 we compare the spectra at the five main emission positions to synthetic spectra based on the temperatures derived from our previous methyl formate analysis. Finally, we discuss in Sect. 5 the similarity in spatial structure and velocity between our high resolution maps of dimethyl ether and methyl formate and examine its implication on the different chemical models of formation of these species, in particular in comparison also with our ethanol and formic acid maps.

## 2. Observations

The data set consists in twelve data cubes obtained with the IRAM Plateau de Bure Interferometer, the parameters of which are presented in Favre et al. (2011a; see their Table 1). We used the GILDAS package<sup>1</sup> for data reduction. The continuum emission was subtracted in the data cubes by selecting line-free channels as judged by careful visual inspection, discarding any contaminated channels. Finally, we cleaned the data cubes, channel by channel, using the B. G. Clark method (Clark 1980).

Table 1 presents the parameters of the four cubes where transitions of dimethyl ether are detected. Spatial resolution ranges from  $1.79'' \times 0.79''$  to  $7.63'' \times 5.35''$  and spectral resolution from 0.84 to 2.33  $\text{km s}^{-1}$ .

**Table 2.** Detected and blended transitions of dimethyl ether observed with the Plateau de Bure Interferometer toward Orion-KL.

Frequency (MHz)	Transition	$E_{\text{up}}$ (K)	$S\mu^2$ (D <sup>2</sup> )	Note <sup>a</sup>
80536.3550	5(2,3)-5(1,4) AE	19.3	32.2	D
80536.4060	5(2,3)-5(1,4) EA	19.3	21.5	D
80538.6540	5(2,3)-5(1,4) EE	19.3	86.0	D
80540.9280	5(2,3)-5(1,4) AA	19.3	53.7	D
80651.6720	21(5,17)-20(6,14) AA	245.8	28.4	B
101559.3870	12(2,10)-11(3,9) AA	77.6	19.6	D
101559.9530	22(5,17)-21(6,16) AA	265.9	30.6	D
101561.3170	22(5,17)-21(6,16) EE	265.9	81.5	D
101562.1200	12(2,10)-11(3,9) EE	77.6	52.3	D
101562.6290	22(5,17)-21(6,16) AE	265.9	10.2	D
101562.7350	22(5,17)-21(6,16) EA	265.9	20.3	D
101564.8330	12(2,10)-11(3,9) AE	77.6	6.5	D
101564.8730	12(2,10)-11(3,9) EA	77.6	13.1	D
203364.0480	3(3,0)-2(2,0) EA	18.1	5.1	B
203374.1550	3(3,1)-2(2,0) EE	18.1	28.1	B
203375.7530	3(3,1)-2(2,0) AE	18.1	8.4	B
203383.0690	3(3,1)-2(2,0) AA	18.1	25.3	B
203384.3710	3(3,0)-2(2,0) EE	18.1	39.3	B
203384.4500	3(3,1)-2(2,0) EA	18.1	11.8	B
203402.7050	3(3,0)-2(2,1) EA	18.1	11.8	B
203410.1000	3(3,1)-2(2,1) EE	18.1	39.3	PB
203411.4020	3(3,0)-2(2,1) AE	18.1	25.3	PB
203418.7180	3(3,0)-2(2,1) AA	18.1	42.2	PB
203420.3160	3(3,0)-2(2,1) EE	18.1	28.2	PB
203423.1070	3(3,1)-2(2,1) EA	18.1	5.1	PB
223409.4660	26(2,24)-26(1,25) EE	330.4	276.7	D
223412.0350	26(2,24)-26(1,25) AA	330.4	103.8	D

<sup>a</sup> D: detected. B: blended. PB: partial blend.

## 3. Dimethyl ether (CH<sub>3</sub>OCH<sub>3</sub>) frequencies and maps

### 3.1. Dimethyl ether frequencies

The data set includes several dimethyl ether (DME) lines. Table 2 lists the DME transitions, present in our data and detected or blended, taken from the CDMS database<sup>2</sup> (Müller et al. 2001, 2005) up to  $E_{\text{upper}} \lesssim 650 \text{ K}$  and based on the recent work of Endres et al. (2009). The non detected transitions correspond to lines too faint to be detected ( $S\mu^2 \geq 6.5$  for the detected transitions and  $S\mu^2 \leq 4.1$  for non detected). The detected transitions cover the energy range 19 to 330 K.

Dimethyl ether is an asymmetric top molecule with two equivalent methyl groups undergoing large amplitude motions along the CO-bond. The two internal rotations cause a splitting

<sup>1</sup> <http://www.iram.fr/IRAMFR/GILDAS>

<sup>2</sup> <http://www.astro.uni-koeln.de/cdms>

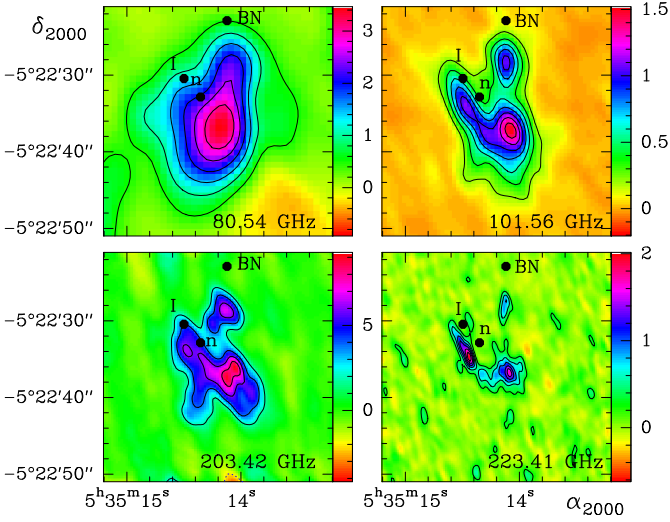


**Fig. 1.** Dimethyl ether integrated intensity maps obtained with the Plateau de Bure Interferometer: these panels show the sum of the emission of the transitions at 80.54 GHz, 101.56 GHz, 203.42 GHz and 223.41 GHz. The first contour and the step are 0.5 Jy/beam, 0.2 Jy/beam, 2 Jy/beam and 0.3 Jy/beam at 80.54 GHz, 101.56 GHz, 203.42 GHz and 223.41 GHz respectively. Note that the 203.42 GHz transitions are blended with the H<sub>2</sub><sup>18</sup>O line at 203.407 GHz around ( $\alpha_{J2000} = 05^h35^m14^s.5$ ,  $\delta_{J2000} = -05^\circ22'34''$ ). The BN object position is ( $\alpha_{J2000} = 05^h35^m14^s.1094$ ,  $\delta_{J2000} = -05^\circ22'22''.724$ ), the radio source I position is ( $\alpha_{J2000} = 05^h35^m14^s.5141$ ,  $\delta_{J2000} = -05^\circ22'30''.575$ ), and the IR source n position is ( $\alpha_{J2000} = 05^h35^m14^s.3571$ ,  $\delta_{J2000} = -05^\circ22'32''.719$ ) from Goddi et al. (2011).

of each rotational level into four substates AA, EE, EA, and AE (see Sect. 4 for line strengths and frequency separation of the multiplets).

### 3.2. The dimethyl ether emission maps

The maps of the dimethyl ether molecule, CH<sub>3</sub>OCH<sub>3</sub>, allow us to trace the spatial distribution of one major oxygenated molecule in Orion-KL. Figure 1 shows the CH<sub>3</sub>OCH<sub>3</sub> emission measured at different wavelengths; note the different angular resolutions of the various data sets (listed in Table 1). The distribution shows the same extended, V-shaped molecular emission linking the radio source I to the BN object as previously observed in methyl formate (Favre et al. 2011a). The highest spatial resolution map at 223.41 GHz (1.79'' $\times$ 0.79'') is presented in Fig. 2. We have marked the Hot Core and Compact Ridge positions (see e.g. Beuther et al. 2005). The position of the main emission peaks identified in methyl formate, labeled MF1 to MF28, are indicated. Most of these correspond to the dimethyl ether peaks as well within the beam size.

The distribution of CH<sub>3</sub>OCH<sub>3</sub> appears very similar to the distribution of HCOOCH<sub>3</sub> in the velocity range where the main component lies between 6 and 9 km s<sup>-1</sup> and a north-south linear structure shows up at higher velocities (9–12 km s<sup>-1</sup>).

The relative intensities of the different spatial emission peaks depend on the upper state energy of the transitions. Figure 3 shows the CH<sub>3</sub>OCH<sub>3</sub> emission for transitions with different energy levels ranging from  $E_{\text{up}}=18$  to 330 K. The 43.47 GHz map is that obtained with the EVLA (Favre et al. 2011b). As previously observed for the methyl formate in Favre et al. (2011a), the emission of dimethyl ether at the MF2 position ("Hot Core SW"

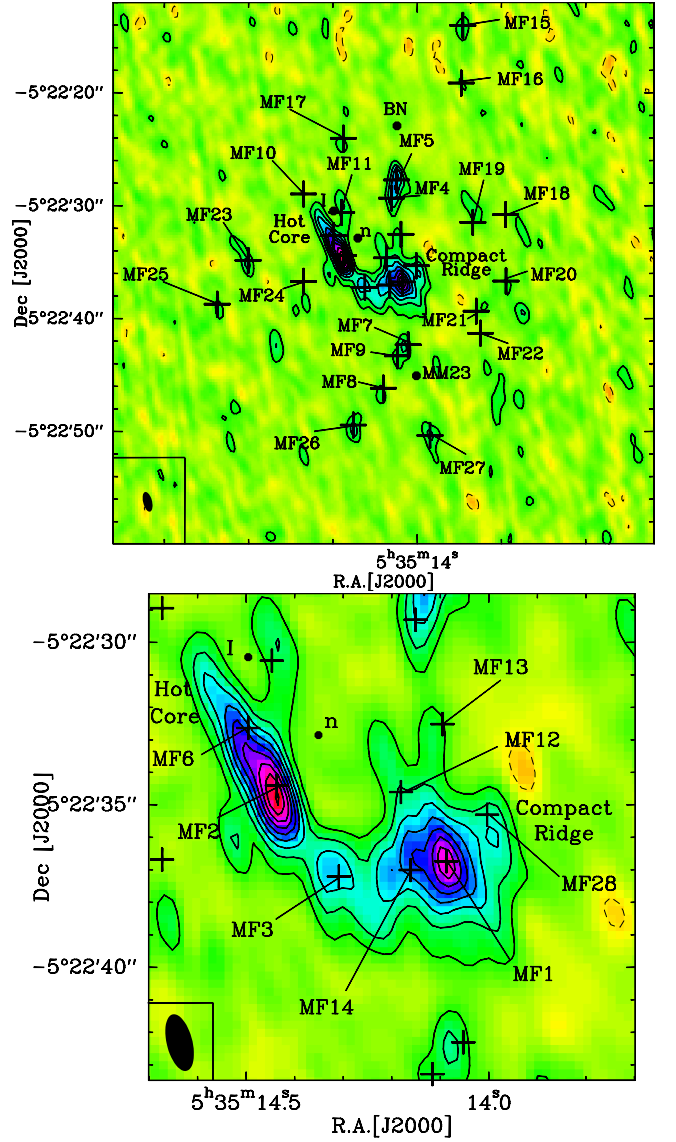


**Fig. 2.** Dimethyl ether integrated intensity maps obtained with the Plateau de Bure Interferometer (sum of emission at 223.409 GHz and 223.412 GHz between 5 and 12 km s<sup>-1</sup>). The bottom image is a blowup of the Hot Core/Compact Ridge map area. The beam is 1.79''  $\times$  0.79''; the level step and first contour are 3.8 K km s<sup>-1</sup>. The position of the millimeter source MM23 (Eisner et al. 2008) is also indicated. The main different HCOOCH<sub>3</sub> emission peaks identified in Favre et al. (2011a) are marked by a cross and labeled MF<sub>NUMBER</sub>. Note that the dimethyl ether distribution is very similar to that of methyl formate (cf. Fig. 4 in Favre et al. 2011a, and see Sect. 5.1.1).

in Friedel & Snyder 2008) becomes stronger at higher energy levels.

The comparison of our interferometric spectrum at 101.56 GHz to the single-dish spectrum taken with the IRAM 30m (J. Cernicharo, private comm.) shows that little flux is missing due to filtering on a 3'' scale (see Fig. 4).

### 4. Temperatures and column densities

The four torsional forms AA, EE, AE and EA have weights of 6:16:2:4 for ee, oo levels and 10:16:4:6 for eo and oe levels (Turner 1991; Lovas et al. 1979). Most of the time the spectral

**Table 3.** Positions of the main HCOOCH<sub>3</sub> emission peaks observed with the Plateau de Bure Interferometer toward Orion-KL as identified in Favre et al. (2011a). These peaks also coincide with the main CH<sub>3</sub>OCH<sub>3</sub> peaks.

Position name	R.A. (J2000) 05 <sup>h</sup> 35 <sup>m</sup>	Dec (J2000) -05°22′
MF1	14:09	36:7
MF2	14:44	34:4
MF3	14:31	37:2
MF4	14:15	29:3
MF5	14:12	27:7

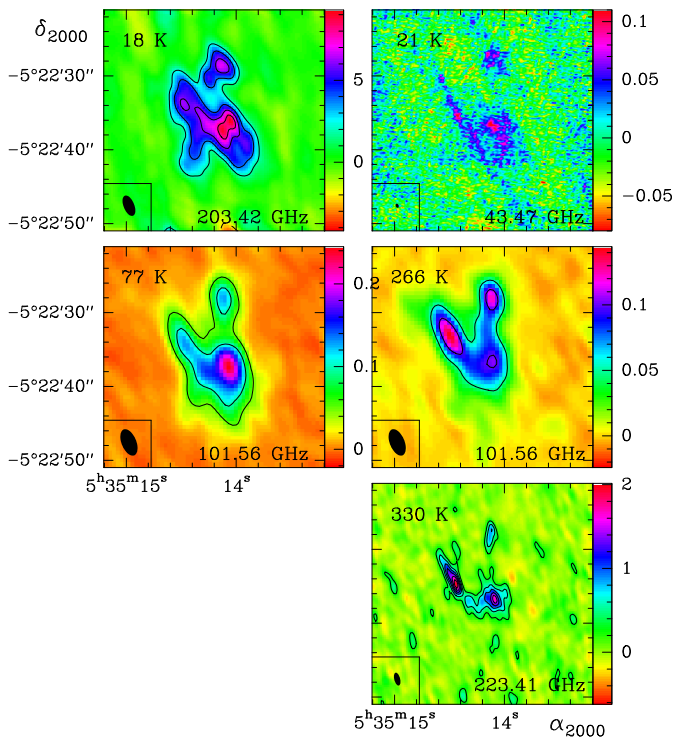


**Fig. 3.** CH<sub>3</sub>OCH<sub>3</sub> intensity maps integrated in velocity between 5 and 12 km s<sup>-1</sup>. The line frequency and the upper state energy are indicated on each plot. The CH<sub>3</sub>OCH<sub>3</sub> 43.47 GHz map was obtained with the EVLA (Favre et al. 2011b). The dimethyl ether emission is stronger towards the compact ridge than the hot core SW position for low upper energy transitions, while the opposite is the case for high upper state energies.

resolution of the radiotelescopes does not allow separation of the AE and EA transitions, so that a symmetrical triplet is observed. In that case and if the lines are optically thin, the observed dimethyl ether triplet (AA, EE, AE+EA) should then be either 6:16:6 or 10:16:10 in relative intensity. For part of the triplet observed at the edge of the bandwidth at 223.4 GHz we find a ratio of 1:2.7:1 within the errors. This is in agreement with a low optical depth. However for the transitions at 80.53 GHz, the EE line in the middle is much too weak with respect to the other lines. This EE line is stronger in the spectra taken with single-dish radiotelescopes (Johansson et al. 1985; Turner 1989), so that this could be caused by an observational rather than an excitation effect.

For the transitions at 101.56, 203.42 and 223.41 GHz, we have produced synthetic spectra assuming local thermodynamic equilibrium (LTE), using the line parameters derived

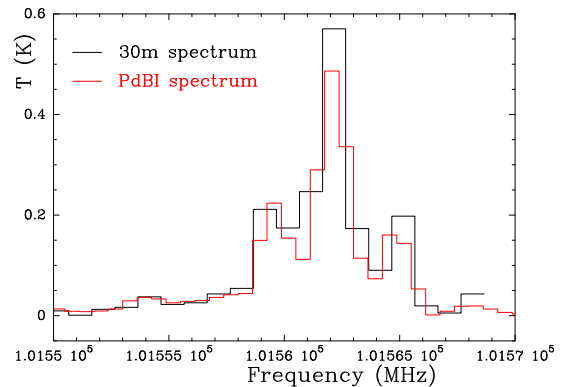


**Fig. 4.** Dimethyl ether spectrum at 101.56 GHz observed with the IRAM 30m radiotelescope (in black, J. Cernicharo, private comm.) overlaid on the PdBI spectrum convolved to the same spatial resolution (in red).

from our methyl formate analysis toward the five main emission peaks whose positions are given in Table 3. We first used the HCOOCH<sub>3</sub> velocity  $v$ , line width  $\Delta v_{1/2}$  and temperature  $T_{\text{rot}}$  to derive the N<sub>CH<sub>3</sub>OCH<sub>3</sub></sub> column density; then we have slightly adjusted the parameters for a better fit of the dimethyl ether spectra. This was done with our own routines and XCLASS<sup>3</sup>. Fig. 5 shows synthetic spectra overlaid on the observed spectra and Table 4 lists the parameters for the angular resolutions of the 101 GHz (3.63'' × 2.26'') and 223 GHz (1.79'' × 0.79'') observations. The parameters used for the 203 GHz observations (angular resolution of 2.94'' × 1.44'') are intermediate values. The calculated opacities (estimated from the ratio of the brightness temperature to the rotational temperature) are generally less than 0.2 and at most 0.4 at MF1.

We derived abundances relative to methanol using the column densities of Peng et al. (2012). We find values between 0.05 and 0.2. This result assumes that both gas components are co-extensive and in LTE at the same temperature, which might be questionable if the difference in the derived temperature between dimethyl ether and methanol is significant. This question is related to the dimethyl ether formation route and is discussed later in Sect. 5.

## 5. Discussion

### 5.1. Similarity of dimethyl ether and methyl formate HCOOCH<sub>3</sub> maps

Most maps of molecular emission in Orion KL obtained in previous studies show a huge diversity in morphology. On the contrary we show here the very striking *similarity* which appears between our high resolution maps of dimethyl ether and methyl formate (Favre et al. 2011a). The high degree of correlation we find reinforces the need to explain the similarity already noted between these species in previous studies, and probably points towards a similarity of their formation paths, with a common precursor for both species.

First we present the correlation of dimethyl ether with methyl formate observed in this work and previous results for these molecules. We then briefly review the models of gas phase

<sup>3</sup> This research made use of the myXCLASS program (<https://www.astro.uni-koeln.de/projects/schilke/XCLASS>), which accesses the CDMS (<http://www.cdms.de>) and JPL (<http://spec.jpl.nasa.gov>) molecular data bases.



**Table 4.** CH<sub>3</sub>OCH<sub>3</sub> synthetic spectra parameters (velocity, line width, beam-averaged temperature and column density) which reproduce best the PdBI spectra at the emission peaks MF1 to MF5 for the angular resolutions of the 101 GHz (3.63'' × 2.26'') and 223 GHz (1.79'' × 0.79'') observations. Two velocities components are clearly distinguished at MF1, MF4 and MF5.

Emission peaks	v (km s <sup>-1</sup> )	Δv <sub>1/2</sub> (km s <sup>-1</sup> )		T <sub>rot</sub> (K)		N <sub>CH<sub>3</sub>OCH<sub>3</sub></sub> (10 <sup>17</sup> cm <sup>-2</sup> )	
		(1.79'' × 0.79'')	(3.63'' × 2.26'')	(1.79'' × 0.79'')	(3.63'' × 2.26'')	(1.79'' × 0.79'')	(3.63'' × 2.26'')
MF1	7.5	1.85	3.0	80	120	3.45	2.7
MF1	9.2	1.0	1.5	120	170	0.15	0.7
MF2	7.7	2.55	4.0	130	125	2.5	2.5
MF3	7.7	2.2	3.7	90	105	1.5	2.0
MF4	8.2–7.6 <sup>a</sup>	2.2	3.5	100	100	0.8	1.5
MF4	11.0	3.0	4.5	100	100	0.3	0.3
MF5	7.35	2.8	3.2	110	110	0.85	1.65
MF5	11.5	3.0	5.0	110	110	0.3	0.45

<sup>a</sup> 8.2 km s<sup>-1</sup> at (1.79'' × 0.79'') and 7.6 km s<sup>-1</sup> at (3.63'' × 2.26'').

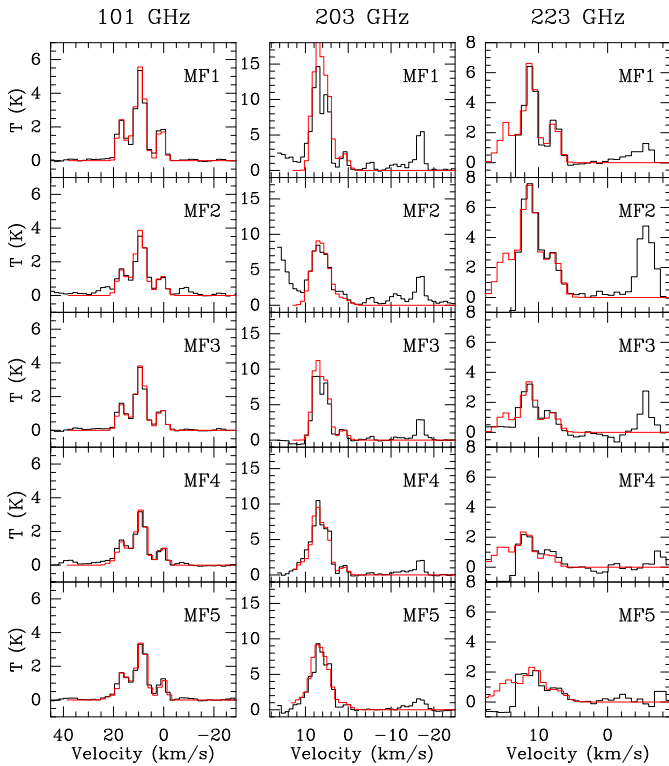


**Fig. 5.** CH<sub>3</sub>OCH<sub>3</sub> synthetic spectra (in red) overlaid on the observed spectra toward the MF1 to MF5 positions. The 101 GHz, 203 GHz and 223 GHz observations are in the left, middle and right columns respectively. The observed spectrum at 223 GHz is at the edge of the bandwidth.

and/or ice mantle chemistry proposed to form these species, concentrating on the most recent works (Laas et al. 2011; Neill et al. 2011; Bisschop et al. 2007; Öberg et al. 2009, 2010) and examine the compatibility of various hypotheses with the present data, as well as with our ethanol and formic acid maps made from the present data set.

#### 5.1.1. PdBI maps and correlation diagrams

When we compare the dimethyl ether map with the methyl formate map obtained with the same data set and from transitions

with close  $E_u$  energies (Fig. 6), these show a striking overall similarity: 1) both molecules are present in the 6–11 km s<sup>-1</sup> velocity range and show no detectable emission at 5 km s<sup>-1</sup>, 2) both molecules show a general V-shaped distribution, 3) they both have their strongest peak at the Compact Ridge for transitions of low  $E_u$  energy range (MF1 position), 4) they both have a second peak (MF2 position) at the position named Hot Core SW by Friedel & Snyder (2008), a few arcseconds below the continuum Hot Core peak, and which is stronger than MF1 for high  $E_u$  energy range transitions (see Sect. 3.2), 5) they both have a northern extension toward BN around 10 km s<sup>-1</sup>, 6) many other secondary peaks are similar.

The correlation between the two maps is however not 100%. Faint emission is present for both species but differ somewhat in shape at other places or is displaced by 1–2''. One should note however the influence of the cleaning procedure necessary to reconstruct the distribution.

The similarity between dimethyl ether and methyl formate maps can be displayed in a more quantitative way. In Fig. 7 the intensity of each pixel of the dimethyl ether emission line ( $E_u=330$  K) at 223.41 GHz and methyl formate emission line ( $E_u=305$  K) at 223.534 GHz are compared (note that there is some correlation between pixels since the pixel size is about 3 times smaller than the synthesized beam). The correlation coefficient of Bravais-Pearson is 0.8. By contrast we show the same type of diagram with formic acid HCOOH (10(2,9)-9(2,8) transition at 223.915 GHz with  $E_u=72$  K) compared to the methyl formate transition at 223.500 GHz (11(4,8)-10(3,7),  $E_u=50$  K) and ethanol C<sub>2</sub>H<sub>5</sub>OH (23(7,17)-23(6,17),  $v_t=0-1$  transition at 223.629 GHz with  $E_u=346$  K) compared to the methyl formate transition at 223.534 GHz (18(5,14)-17(5,13),  $E_u=305$  K), for which the correlation coefficients are only 0.32 and 0.19 respectively. For reference, we also show the correlation of 2 transitions of methyl formate with same energy (223.465 GHz and 223.500 GHz with  $E_u=50$  K); the correlation coefficient is 0.82 – the methyl formate/dimethyl ether result is almost as high. The correlation of 2 transitions of methyl formate with different energies (223.465 GHz and 223.534 GHz with  $E_u=50$  K and 305 K, respectively) is not as good (correlation coefficient of 0.76) due to differences in excitation which are apparent in Fig. 3 and in Favre et al. (2011a, see their Fig. 15). The estimated opacity for all the above transitions is less than 0.15, so that there is no noticeable optical depth effect.

This similarity of the dimethyl ether map with the methyl formate map is not observed with other species (see e.g. Guélin et al. 2008, and our Fig. 8 for formic acid HCOOH).

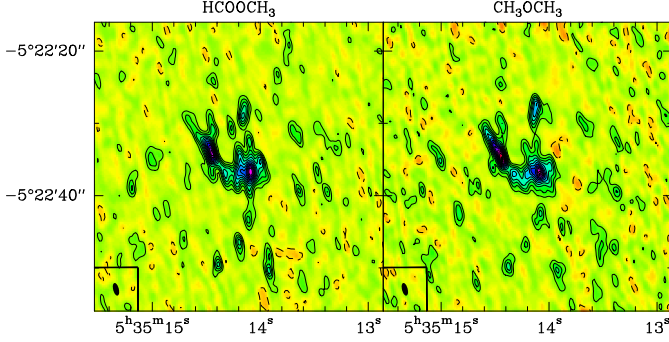


**Fig. 6.** Comparison of the methyl formate map (left) at 223.534 GHz ( $E_u=305$  K) and the dimethyl ether map (right) at 223.41 GHz ( $E_u=330$  K). The transitions are from the same data cube and the  $1.79'' \times 0.79''$  beam is plotted in the bottom left corner.

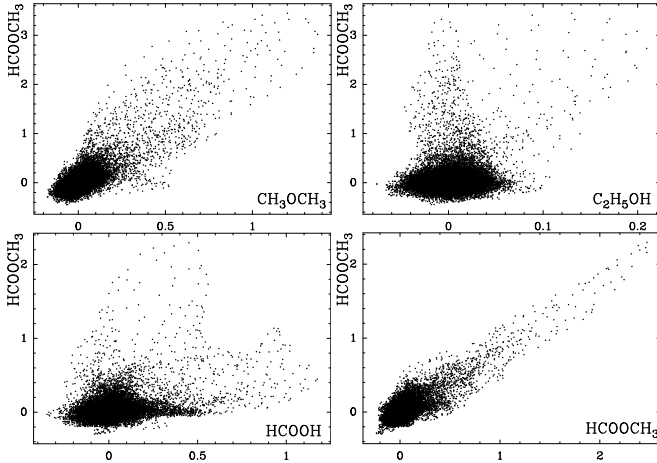


**Fig. 7.** A plot of the intensity of pixels in the methyl formate maps versus the intensity of the same pixels in the dimethyl ether (top left), ethanol (top right), formic acid (bottom left) and methyl formate (bottom right) maps. Care has been taken to use transitions with similar  $E_u$  energies. The methyl formate ( $E_u=305$  K) at 223.534 GHz is compared to the dimethyl ether transition ( $E_u=330$  K) at 223.41 GHz and to the ethanol transition ( $E_u=346$  K) at 223.629 GHz. The methyl formate transition ( $E_u=50$  K) at 223.500 GHz is compared to the formic acid transition ( $E_u=72$  K) at 223.915 GHz and to the methyl formate transition ( $E_u=50$  K) at 223.465 GHz. Dimethyl ether shows clearly the highest spatial correlation with methyl formate.

### 5.1.2. Dimethyl ether and methyl formate behavior in previous publications

The similarity in the distribution between the two species has also been seen in single dish studies of Orion and of other regions. In Table 5 we selected only some of the numerous Orion

KL line surveys based on two factors: 1) early papers from which the parallel between some species so called "compact ridge species", and in some cases already the parallel dimethyl ether/methyl formate distribution, was progressively recognized with increasing evidence, and 2) papers providing the best line profile parameters, temperatures and column densities for both dimethyl ether and methyl formate.

When we convolve our PdBI dimethyl ether data to a typical single-dish field of view of  $30''$ , the spectra can be relatively well fitted with one component of temperature  $T_{\text{rot}} \sim 90$  K and column density  $N_{\text{CH}_3\text{OCH}_3} \sim 0.6 \times 10^{16} \text{cm}^{-2}$ .

Using  $M_X = 4.64 \times 10^{-10} \times \mu_X \times \frac{N_X}{10^{16} \text{cm}^{-2}} \times \left(\frac{\theta}{\text{arcsec}}\right)^2 \times \left(\frac{d}{414 \text{pc}}\right)^2$  to convert the column density of molecule X (averaged over a beam of diameter  $\theta$ ) into a mass  $M_X$  (in solar mass  $M_\odot$ ), we find for dimethyl ether ( $\mu_X = 46$ ):  $M_{\text{DME}} \sim 8.6 \times 10^{-6} M_\odot$ , or about  $2.8 M_{\text{Earth}}$ .

To better compare our results with the single dish studies, we have computed the dimethyl ether mass in each case, and we display the value, R, relative to our result, in column 9 of Table 5. All values are within a factor of two with respect to ours except in the case of the Lee & Cho (2002) observations. No trend is seen with respect to the beam size, despite the large range of sizes; this implies that at least 50%, and perhaps almost all of the dimethyl ether seen in the ODIN wide beam ( $2.1'$ ) is in fact contained in the inner  $30''$  which we have observed with the PdBI. There is no noticeable effect either related to the range of upper level  $E_u$  used in the various studies.

The parallel between both molecules is especially striking on small scales in the present PdBI data. Previous interferometric papers showed some hints of this tendency. Minh et al. (1993) present the first HCOOCH<sub>3</sub> and CH<sub>3</sub>OCH<sub>3</sub> maps, made with the NMA ( $5''.2 \times 4''.2$  resolution); they noted that the difference between the emission distributions of the two molecules may be due to the 100 K difference in upper energy of the observed transition levels. Blake et al. (1996) with OVRO at 1.3 mm ( $1''.5 \times 1''.0$  synthesized beam, and 1 MHz = 1.3 km/s spectral resolution) observed 18 species including methanol, methyl formate and dimethyl ether. No maps are shown for dimethyl ether, but there is a general trend to behave somewhat like HCOOCH<sub>3</sub>, CH<sub>3</sub>OH, H<sub>2</sub>CS and H<sub>2</sub>CO. Beuther et al. (2005, 2006) show many maps obtained with the SMA at 0.86 mm and 0.44 mm of O-bearing species including dimethyl ether, methanol and methyl formate, but at different excitation levels and there is only a partial similarity of the maps. In their CARMA observations at 1.3 mm ( $2''.5 \times 0''.85$ ), Friedel & Snyder (2008) observed both dimethyl ether (transition at  $E_u=81$  K) and methyl formate (transition at  $E_u=120$  K). The maps of the two species did not match perfectly, one peaking at IRc5 and the other at IRc6, but the CH<sub>3</sub>OCH<sub>3</sub> line is blended and a blend with an N-bearing molecule would explain the observed strong emission at IRc6 and the Hot Core SW. Note also that no methyl formate is attributed to the Compact Ridge (while it is the strongest methyl formate peak in Favre et al. 2011a); but these authors define the Compact Ridge position differently. The correlation is very clear in Fig. 3 of Neill et al. (2011) from their CARMA observations; the  $6''.1 \times 5''.0$  resolution is however insufficient to clearly separate the emission from the many individual methyl formate peaks.

**Table 5.** Dimethyl ether and methyl formate parameters from previous single-dish studies.

Authors	Telescope	Beam ( $''$ )	Frequency (GHz)	Dimethyl ether		Methyl formate		R <sup>a</sup>	Comment
				T <sub>rot</sub> (K)	N (10 <sup>16</sup> cm <sup>-2</sup> )	T <sub>rot</sub> (K)	N (10 <sup>16</sup> cm <sup>-2</sup> )		
Goddi et al. (2009)	GBT	16	43	88	5.8			1.07	<sup>b</sup>
Johansson et al. (1984)	Onsala 20m	47	72-90	75	0.25	25-90	0.05-0.25	1.02	
Turner (1991)	NRAO 11m	83	75-115	91	0.13	62	0.66	1.66	<sup>c</sup>
Lee & Cho (2002)	TRAO 14m	46	138-164	130-360	0.5-3.6	55-120	0.6-4.4	2-14	
Remijan et al. (2008)	NRAO 12m	43	130-170	75	0.6			2.05	
Ziurys & McGonagle (1993)	FCRAO 14m	40	150-160	109	0.3	52	0.077	0.89	
Blake et al. (1987)	OVRO 10.4m	30	215-263	63±5	0.3	90±10	0.26	0.50	
Sutton et al. (1995)	JCMT	14	334-343	75	1.49	105	2.45	0.54	<sup>d</sup>
Schilke et al. (1997)	CSO	20	325-360	89±5	1.8	98±3	1.5	1.33	
Schilke et al. (2001)	CSO	11	607-725	360	3	316	13	0.67	
Comito et al. (2005)	CSO	11	795-903	160	2			0.45	
Persson et al. (2007)	Odin satellite	2.1'	486-492/541-577	112	13			0.73	<sup>e</sup>
This paper <sup>f</sup>	PdBI	30	101/203/223	90	0.6			1	<sup>f</sup>

<sup>a</sup> Normalized number of dimethyl ether molecules, see Sect. 5.1.2.

<sup>b</sup> Assuming a 10'' source size.

<sup>c</sup> a second cooler (T<sub>rot</sub>= 22 K) component is seen in MF only with a lower column density (2.7 10<sup>14</sup>).

<sup>d</sup> Compact Ridge position.

<sup>e</sup> Adopted source size 5-6''.

<sup>f</sup> Our PdBI data convolved to a field of view of 30''.

### 5.1.3. The abundance correlation of dimethyl ether with methyl formate

Another important input is the value of the relative dimethyl ether/methyl formate abundances. Table 6 lists the abundances derived at the main positions in our maps for dimethyl ether with respect to methyl formate. Dimethyl ether is about 3–4 times more abundant than methyl formate towards MF3, MF4 and MF5.

Several hypotheses can be considered to explain this correlation:

- Dimethyl ether and methyl formate would emit at the same location because of a similar excitation of the transitions, i.e. a similar behavior with respect to temperature, density or IR radiation field. But there is no special similarity in the level structure of dimethyl ether and methyl formate, especially as compared to other complex organics like ethanol. Furthermore, the physical parameters are not uniform over Orion KL: the temperature varies from 80 to 160 K for methyl formate, which affects the dimethyl ether/methyl formate line ratio. The critical densities are  $\sim 10^{5-8}$  cm<sup>-3</sup> and  $\sim 10^{4-7}$  cm<sup>-3</sup> respectively, while n<sub>H<sub>2</sub></sub> varies from 10<sup>4</sup> to 10<sup>8</sup> cm<sup>-3</sup>. And the IR absorption bands are different, only the CH<sub>3</sub>-O bond is common.
- These molecules are just undergoing sublimation at the same temperature. This is likely, but similar abundances in the ices are also required in that case.
- The similar column densities reflect only the general structure of Orion KL. However dust and other molecules have different patterns.

This leaves a correlation of the molecular abundances in the gas phase as the most simple and likely explanation (see further discussion in Sect. 5.2).

**Table 6.** CH<sub>3</sub>OCH<sub>3</sub> abundance relative to HCOOCH<sub>3</sub> at the emission peaks MF1 to MF5 for the angular resolutions of the 101 GHz (3.63'' × 2.26'') and 223 GHz (1.79'' × 0.79'') observations. We used the N<sub>HCOOCH<sub>3</sub></sub> values listed in Favre et al. (2011a).

Emission peaks	N <sub>CH<sub>3</sub>OCH<sub>3</sub></sub> /N <sub>HCOOCH<sub>3</sub></sub> (1.79'' × 0.79'')   (3.63'' × 2.26'')	
MF1 <sup>a</sup>	2.15	9
MF1 <sup>b</sup>	0.22	4
MF2	1.6	3.5
MF3	3.3	3.6
MF4		4
MF5		3.6

<sup>a</sup> Component at 7.5 km s<sup>-1</sup>.

<sup>b</sup> Component at 9.2 km s<sup>-1</sup>.

### 5.1.4. Dimethyl ether and methyl formate observations in other regions

Single dish observations of several other sources have also noted the parallel between these two species.

In their study of 7 massive hot core regions spread across the Galaxy, Bisschop et al. (2007) study the statistical correlation between the abundances of 13 organic molecules looking for evidence of grain surface chemistry. Methyl formate and dimethyl ether are mostly seen where T<sub>dust</sub> is > 100 K. A strong correlation is found between the abundances of H<sub>2</sub>CO, CH<sub>3</sub>OH, C<sub>2</sub>H<sub>5</sub>OH, HCOOCH<sub>3</sub> and CH<sub>3</sub>OCH<sub>3</sub> and the correlation is even > 0.9 among the last three.

Comparing the results of Bisschop et al. (2007) with our findings, we note that 1) if dimethyl ether appears to be strongly correlated with methyl formate, the correlation they observed is similarly high with ethanol, 2) T<sub>rot</sub> has a large scatter among sources of dimethyl ether, and in some sources may be lower or higher than for methyl formate. Beyond possible observational uncertainties (noise and confusion), one should note the differ-

ent scales of both studies: while we sample down to (1.79'' × 0.79'' or ~500 AU) in the nearby Orion region with the PdB interferometer, the single dish results of Bisschop et al. (2007) are average values for the whole region at Tdust > 100 K which is 1500-5300 AU in radius for their sources - the latter would correspond to a study of Orion over ~20'' in diameter, i.e. most of the KL region. This would explain why ethanol is not distinguished from dimethyl ether and methyl formate, and the less tight correlation between dimethyl ether and methyl formate could be due to additional formation pathways/excitation conditions for a fraction of these species on a larger scale. In other words, the process of formation of methyl formate and dimethyl ether we observe in our case, probably linked to shocks, might not appear as "pure" and unique on a larger scale.

It is interesting to note that in a recent multi-species interferometric study of the young binary protostar IRAS16293, Jørgensen et al. (2011) have mapped CH<sub>3</sub>OCH<sub>3</sub> and HCOOCH<sub>3</sub>. The two molecules appear to be similar, showing two small concentrations of similar intensity around the A and B source components.

An extensive study of O-bearing species was performed in the Galactic Center clouds by Requena-Torres et al. (2006, 2008) which led them to conclude to a "universal" mantle composition in the various GC clouds; this composition is different in hot corinos (Requena-Torres et al. 2006) and in Hot Cores (Requena-Torres et al. 2008). They relate the gas phase abundances of these complex organic molecules to sputtering or evaporation due to shocks, a situation similar to some extent to Orion KL. In the 2006 study, 7 lines of methyl formate and 2 of dimethyl ether were observed, with E<sub>u</sub>/k in the same 20-40 K range; dimethyl ether was not observed in their 2008 study. Note that the rotational temperatures derived in the 2008 study are rather cold (<15 K). Due to the large distance of the GC clouds the sources they observe are likely more extended than what we observe in Orion. These authors do not put any emphasis on the dimethyl ether/methyl formate comparison, although the two molecules are noted to have similar abundances with respect to methanol. The grain surface scheme proposed (Fig. 9 in Requena-Torres et al. 2008) does not suggest any close relation between methyl formate and dimethyl ether.

## 5.2. Formation of dimethyl ether and methyl formate

### 5.2.1. Chemical models

Since detailed presentations can be found elsewhere (e.g. Peeters et al. 2006; Neill et al. 2011; Herbst & van Dishoeck 2009) we summarize here only briefly different models.

A first model of pure gas-phase ion-molecule chemistry was proposed (e.g. Blake 1988) where the protonated methanol ion, CH<sub>3</sub>OH<sub>2</sub><sup>+</sup>, produced both CH<sub>3</sub>OCH<sub>3</sub> and HCOOCH<sub>3</sub>, through reactions with CH<sub>3</sub>OH and H<sub>2</sub>CO respectively, which naturally explained the suspected intimate chemical link between these species. However, a first difficulty for an interstellar chemistry model is to produce a sufficient amount of these complex species. The pure ion-molecule chemistry proved unable to produce the observed abundances. This led to suggest a role of surface chemistry and of the release of mantle molecules into the gas phase by some process. The models considered first injection of water, but injection of methanol itself, processed once in the gas phase by ion-molecule chemistry appeared to be required. A key species in this scheme remained protonated methanol CH<sub>3</sub>OH<sub>2</sub><sup>+</sup>, and a close correlation of methyl formate and dimethyl ether was predicted (e.g. Charnley et al. 1995;

Caselli et al. 1993). Most of the more complex species predicted to be abundant by the Charnley et al. (1995) model remain undetected, although one of these (not expected to be the most abundant one), ethyl formate HCOOC<sub>2</sub>H<sub>5</sub>, has recently been detected in Sgr B2 (Belloche et al. 2009). This ice mantle methanol release/gas-phase post-processing model could not produce enough methyl formate when calculations by Horn et al. (2004) showed that the reaction CH<sub>3</sub>OH<sub>2</sub><sup>+</sup> + H<sub>2</sub>CO was not possible at interstellar temperatures.

Presently there are two different proposals: 1) new gas-phase ion-molecule formation routes where formaldehyde is replaced by formic acid (e.g. Neill et al. 2011); 2) a direct formation of methyl formate and dimethyl ether on the grains (e.g. Garrod et al. 2008; Laas et al. 2011).

### 5.2.2. How do these models confront our Orion dimethyl ether and methyl formate data

In our view, the simplest and most natural explanation of the dimethyl ether-methyl formate correlation is the production of both species by a common precursor reacting with an abundant simple species such as either CH<sub>3</sub>OH, H<sub>2</sub>CO or HCOOH. However, we suggest another - less likely in our view - possibility: the convergence of the dimethyl ether and methyl formate abundances resulting from the long time evolution of many chemical reactions.

The common precursor hypothesis: CHO radical (solid phase) vs CH<sub>3</sub>OH and CH<sub>3</sub>OH<sub>2</sub><sup>+</sup> (gas phase)

If solid phase chemistry dominates, the common precursor would be the CH<sub>3</sub>O radical, as detailed in Öberg et al (2010). In the scheme of UV irradiated ices, photodissociation of CH<sub>3</sub>OH leads to two radicals CH<sub>3</sub>O and CH<sub>2</sub>OH<sup>4</sup>. The former is the precursor of methyl formate and dimethyl ether which are formed respectively by reaction with HCO and CH<sub>3</sub> on the grain. The other radical produced from methanol, CH<sub>2</sub>OH, leads to ethanol C<sub>2</sub>H<sub>5</sub>OH, ethylene glycol CH<sub>2</sub>OHCH<sub>2</sub>OH and glycolaldehyde CH<sub>2</sub>OHCHO. A strong prediction of this model would thus be that the 3 latter molecules should show a somewhat similar distribution, which is likely to be different from that of methyl formate and dimethyl ether. Different conditions, either in the pre-explosion phase (a preencounter role of BN, distance to the Trapezium, different heating, e.g. due to the proximity of source

<sup>4</sup> The mantle chemistry scheme needs UV radiation to produce radicals. Is it possible in Orion KL? According to our previous study on deuterated methanol (Peng et al. 2012), the composition of ice mantles might have been largely determined in an earlier phase of the cloud, well before the explosive event. During this earlier phase, the matter was conceivably more uniform and less dense, hence less opaque to UV. The present very high opacity of the cloud (up to A<sub>v</sub> > 1000, Favre et al. 2011a) suggests that processing by external UV sources is now negligible except on a very thin external layer. Inside a dense cloud UV can also be produced by dissociative shocks (e.g. Neufeld & Dalgarno 1989) or by secondary electrons (e.g. Gredel et al. 1989; Prasad & Tarafdar 1983). The presence of at least one B star inside Orion KL (the BN object) could also be an internal UV source but which is unlikely to reach the compact ridge due to absorption. However, as we have no knowledge of the precise 3D structure of the cloud, we cannot completely exclude that there are holes in the gas and we ignore the 3D dust distribution within Orion-KL. But the simplest origin for the UV mantle irradiation remains that it occurred at an earlier epoch. Note that radicals can be formed also in mantles also by irradiation by charged particles (see e.g. Bennett & Kaiser 2007; Herbst & van Dishoeck 2009).



I), or after the explosive event (direct effect of the shock, or subsequent exposure to the photons of BN, even higher proximity of IR luminous source I) might explain the different importance of the CH<sub>2</sub>OH and CH<sub>3</sub>O molecules in the Hot Core and in the Compact Ridge. Indeed, our interferometric observations show a similar distribution for C<sub>2</sub>H<sub>5</sub>OH and CH<sub>2</sub>OHCH<sub>2</sub>OH but different from that of HCOOCH<sub>3</sub> and CH<sub>3</sub>OCH<sub>3</sub> (Guélin et al. 2008, Brouillet et al. in prep.); however, CH<sub>2</sub>OHCHO is not detected (Favre et al. 2011a). Note that some conversion mechanisms between CH<sub>2</sub>OH and CH<sub>3</sub>O are suggested by Cernicharo et al. (2012) in their CH<sub>3</sub>O detection paper.

If the molecules would be mainly produced in the gas phase, methyl formate could be produced from formic acid as suggested by Neill et al. (2011): the anti-correlation observed between HCOOH and HCOOCH<sub>3</sub> across most of the Orion-KL region (see Fig. 8) is consistent with their model of recent gas-phase conversion. Two ion–molecule reactions involving the reaction of methanol and formic acid, where one of the reactants is protonated, could be viable interstellar reaction routes to form methyl formate. Either the methanol, CH<sub>3</sub>OH, or the protonated methanol, CH<sub>3</sub>OH<sub>2</sub><sup>+</sup>, would then be the common precursor to methyl formate and dimethyl ether. Indeed, the reaction between protonated methanol and neutral methanol produces protonated dimethyl ether and is considered as an important contributor to interstellar dimethyl ether formation. If methyl formate is efficiently produced in a region by the reaction between HCOOH and CH<sub>3</sub>OH<sub>2</sub><sup>+</sup>, dimethyl ether is produced as well in the same spatial region, since neutral methanol is also present. A prediction of these reactions is the presence of the less stable t-HCOOCH<sub>3</sub>, which is not yet detected in Orion, and the anti-correlation with HCOOH, consumed by the reaction. Another interesting test would be to detect directly CH<sub>3</sub>OH<sub>2</sub><sup>+</sup>, once its millimetric spectrum is known.

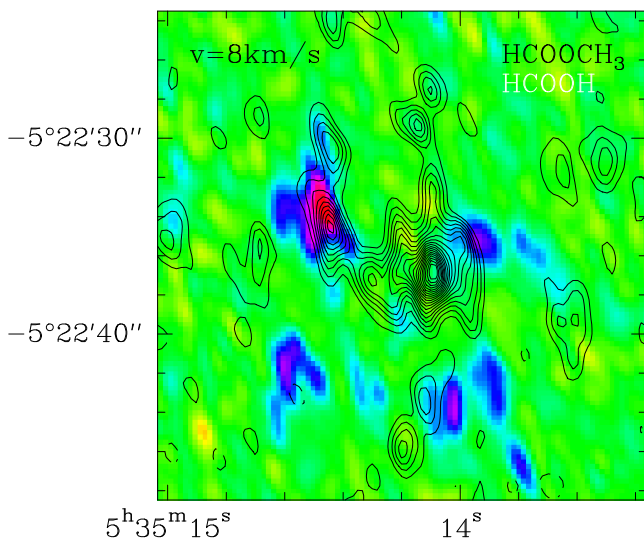


**Fig. 8.** Methyl formate channel map (black contours) at 8 km s<sup>-1</sup> (sum of the transitions at 223.465 and 223.500 GHz,  $E_u=50$  K) overlaid on the formic acid channel map (colors) at the same velocity for the 223.915 GHz transition ( $E_u=72$  K). All data are taken from the same data set (1.79'' × 0.79'' resolution).

Methanol maps (see maps in Peng et al. 2012, from the same data set) are somewhat different. Despite the fact methyl

formate and dimethyl ether are chemically related to CH<sub>3</sub>OH, their distributions are not expected to correlate as tightly with methanol as with each other since: i) in the gas phase production scheme, the methyl formate/dimethyl ether precursor CH<sub>3</sub>OH<sub>2</sub><sup>+</sup> can be produced with an efficiency varying across Orion-KL. In addition CH<sub>3</sub>OH, as the parent species, is partly consumed to some extent (5-20%) to form methyl formate and dimethyl ether (and could have other reactions); ii) in the ice mantle production scheme, some layering of the mantle is expected (see e.g. Herbst & van Dishoeck 2009), and only a fraction of solid methanol closest to the surface can be processed by UV.

We suggest, however, another possibility which could be investigated for the gas-phase chemistry. Because the main problem to form HCOOCH<sub>3</sub> from CH<sub>2</sub>OH<sub>2</sub><sup>+</sup> and H<sub>2</sub>CO is an energy barrier, could this obstacle be removed if one considers that the ions are strongly accelerated with respect to neutrals at some places of an MHD shock? A few km/s would represent enough kinetic energy to overcome the reaction barrier, which is 128 kJ/mol (15 000 K or 1.2 eV) according to Horn et al. (2004). New quantum calculations and/or laboratory work are required to test this hypothesis.

An alternative hypothesis could be: convergence of methyl formate and dimethyl ether abundances with time.

We cannot exclude the convergence with time of the chemical network to a same methyl formate/dimethyl ether ratio value for a large range of initial conditions and parameters. (Note that such a convergence is not always present; for instance chemical systems may oscillate.) No common precursor is needed in this case. The convergence should be achieved in a time short enough (at least < 1-10 Myr, the probable maximum age of molecular clouds in OMC 1). This hypothesis is less likely in our view (cf the probable consequences of recent shocks).

## 6. Conclusions

We have studied the distribution of the complex O-bearing molecule dimethyl ether CH<sub>3</sub>OCH<sub>3</sub> at medium and high angular resolution (6.5'' – 1'') using various sets of interferometric data from the IRAM Plateau de Bure Interferometer. Our main results and conclusions are the following:

1. This data set includes 4 well detected lines from  $E_u=19$  K to  $E_u=330$  K and other partially blended or blended lines.
2. The most intense emission arises from the Compact Ridge at the methyl formate peak position (MF1, Favre et al. 2011a); the second most intense at the Hot Core SW position (Friedel & Snyder 2008) or MF2 (Favre et al. 2011a).
3. We have used the temperature derived from our previous methyl formate study for the five main peaks and we have deduced CH<sub>3</sub>OCH<sub>3</sub> column densities assuming LTE. Temperatures cover the range 80 to 170 K, and column densities 1.5 × 10<sup>16</sup> to 3.5 × 10<sup>17</sup> cm<sup>-2</sup>.
4. The abundance of CH<sub>3</sub>OCH<sub>3</sub> relative to methanol, CH<sub>3</sub>OH, is in the range 0.05 to 0.2 depending on the positions and assuming identical spatial distribution and temperature for both molecules. When observed on the same spatial scale of 3.6'' × 2.3'', the abundance of CH<sub>3</sub>OCH<sub>3</sub> relative to methyl formate, HCOOCH<sub>3</sub>, is in the range 3.5 to 9.
5. We observe a very good correlation of the spatial distribution of the methyl formate and dimethyl ether emission. We show that it is most likely due to a correlation of their abundances.

6. The dimethyl ether emission follows the 2.12  $\mu\text{m}$  H<sub>2</sub> distribution, as does the methyl formate distribution. Shocks seem to be related to the presence of these species, possibly because of the release of molecules from grain mantles.
7. A common precursor to dimethyl ether and methyl formate appears the simplest explanation to the observed correlation. In the gas phase, the precursor CH<sub>3</sub>OH<sub>2</sub><sup>+</sup> would react respectively with CH<sub>3</sub>OH and, as suggested by Neill et al. (2011), with HCOOH. The reaction of protonated methanol CH<sub>3</sub>OH<sub>2</sub><sup>+</sup> with H<sub>2</sub>CO and CH<sub>3</sub>OH is excluded by quantum calculations in normal interstellar conditions. We speculate whether the reaction of high speed CH<sub>3</sub>OH<sub>2</sub><sup>+</sup> ions (a few km/s to > 20 km/s) might change this conclusion. On the other hand, if methyl formate and dimethyl ether are already produced in the ice mantle, CH<sub>3</sub>OH and/or methoxy radical CH<sub>3</sub>O seem to be the common precursor.
8. We observe a different distribution of ethanol C<sub>2</sub>H<sub>5</sub>OH (and ethylene glycol CH<sub>2</sub>OHCH<sub>2</sub>OH, in prep.). In the grain mantle chemistry scheme this could result from different production rates or schemes of CH<sub>2</sub>OH vs CH<sub>3</sub>O radicals across Orion-KL. Furthermore we confirm the anti-correlation of methyl formate with formic acid, HCOOH, found by Neill et al. (2011). This in favor of their model of production of methyl formate from gas phase HCOOH and CH<sub>3</sub>OH<sub>2</sub><sup>+</sup> where CH<sub>3</sub>OH<sub>2</sub><sup>+</sup> is formed from methanol released from grains.

High resolution mapping brings new insight to the comparison of complex organic molecules and the understanding of their formation. The HCOOCH<sub>3</sub> and CH<sub>3</sub>OCH<sub>3</sub> tight correlation, and the different behavior of ethanol we observe are a strong constraint for future chemical models.

We identify the need for the following key studies to constrain further the chemistry of dimethyl ether and O-bearing complex species: search for mantle species produced by the CH<sub>2</sub>OH radical; search for CH<sub>3</sub>OH<sub>2</sub><sup>+</sup>; maps of t-HCOOCH<sub>3</sub> and HCOOH; theoretical/laboratory studies of protonated methanol reaction at high speed (shocked) on H<sub>2</sub>CO and CH<sub>3</sub>OH. The conditions leading to the convergence of the dimethyl ether/methyl formate ratio in a complex chemical network could also be investigated.

Shock related molecule release from grains and shock induced chemistry of complex molecules need to be modeled. The issue of the efficiency or lack of such chemical conditions to transform molecules in a short time lapse (<10<sup>3</sup> yr) is critical in the discussion of the merits of the two methyl formate and dimethyl ether production schemes (gas phase production vs simple release); this will be addressed in a future work.

*Acknowledgements.* This research has made use of the SIMBAD database, operated at the CDS, Strasbourg, France, and of the Splatalogue database (<http://www.splatalogue.net>, Remijan et al. 2007). This work was supported by the CNRS national programs PCMI (Physics and Chemistry of the Interstellar Medium) and GDR Exobiology. We thank J. Cernicharo for his IRAM 30m spectra. We thank the referee and the editor for raising interesting issues.

## References

- Allen, D. A. & Burton, M. G. 1993, *Nature*, 363, 54  
 Belloche, A., Garrod, R. T., Müller, H. S. P., et al. 2009, *A&A*, 499, 215  
 Bennett, C. J. & Kaiser, R. I. 2007, *ApJ*, 661, 899  
 Beuther, H., Zhang, Q., Greenhill, L. J., et al. 2005, *ApJ*, 632, 355  
 Beuther, H., Zhang, Q., Reid, M. J., et al. 2006, *ApJ*, 636, 323  
 Bisschop, S. E., Jørgensen, J. K., van Dishoeck, E. F., & de Wachter, E. B. M. 2007, *A&A*, 465, 913  
 Blake, G. A. 1988, in *Lecture Notes in Physics*, Berlin Springer Verlag, Vol. 315, *Molecular Clouds, Milky-Way and External Galaxies*, ed. R. L. Dickman, R. L. Snell, & J. S. Young, 132  
 Blake, G. A., Mundy, L. G., Carlstrom, J. E., et al. 1996, *ApJ*, 472, L49+  
 Blake, G. A., Sutton, E. C., Masson, C. R., & Phillips, T. G. 1987, *ApJ*, 315, 621  
 Caselli, P., Hasegawa, T. I., & Herbst, E. 1993, *ApJ*, 408, 548  
 Cernicharo, J., Marcelino, N., Roueff, E., et al. 2012, *ApJ*, 759, L43  
 Charnley, S. B., Kress, M. E., Tielens, A. G. G. M., & Millar, T. J. 1995, *ApJ*, 448, 232  
 Clark, B. G. 1980, *A&A*, 89, 377  
 Clark, F. O., Lovas, F. J., & Johnson, D. R. 1979, *ApJ*, 229, 553  
 Comito, C., Schilke, P., Phillips, T. G., et al. 2005, *ApJS*, 156, 127  
 Eisner, J. A., Plambeck, R. L., Carpenter, J. M., et al. 2008, *ApJ*, 683, 304  
 Endres, C. P., Drouin, B. J., Pearson, J. C., et al. 2009, *A&A*, 504, 635  
 Favre, C., Despois, D., Brouillet, N., et al. 2011a, *A&A*, 532, 32  
 Favre, C., Wootten, H. A., Remijan, A. J., et al. 2011b, *ApJ*, 739, L12  
 Friedel, D. N. & Snyder, L. E. 2008, *ApJ*, 672, 962  
 Garrod, R. T., Weaver, S. L. W., & Herbst, E. 2008, *ApJ*, 682, 283  
 Goddi, C., Greenhill, L. J., Humphreys, E. M. L., et al. 2009, *ApJ*, 691, 1254  
 Goddi, C., Humphreys, E. M. L., Greenhill, L. J., Chandler, C. J., & Matthews, L. D. 2011, *ApJ*, 728, 15  
 Gómez, L., Rodríguez, L. F., Loinard, L., et al. 2005, *ApJ*, 635, 1166  
 Gredel, R., Lepp, S., Dalgarno, A., & Herbst, E. 1989, *ApJ*, 347, 289  
 Guélin, M., Brouillet, N., Cernicharo, J., Combes, F., & Wooten, A. 2008, *Ap&SS*, 313, 45  
 Herbst, E. & van Dishoeck, E. F. 2009, *ARA&A*, 47, 427  
 Hirota, T., Bushimata, T., Choi, Y. K., et al. 2007, *PASJ*, 59, 897  
 Horn, A., Møllendal, H., Sekiguchi, O., et al. 2004, *ApJ*, 611, 605  
 Johansson, L. E. B., Andersson, C., Elder, J., et al. 1985, *A&AS*, 60, 135  
 Johansson, L. E. B., Andersson, C., Elder, J., et al. 1984, *A&A*, 130, 227  
 Jørgensen, J. K., Bourke, T. L., Nguyen Luong, Q., & Takakuwa, S. 2011, *A&A*, 534  
 Kim, M. K., Hirota, T., Honma, M., et al. 2008, *PASJ*, 60, 991  
 Laas, J. C., Garrod, R. T., Herbst, E., & Widicus Weaver, S. L. 2011, *ApJ*, 728, 71  
 Lee, C. W. & Cho, S.-H. 2002, *Journal of Korean Astronomical Society*, 35, 187  
 Lovas, F. J., Johnson, D. R., & Snyder, L. E. 1979, *ApJS*, 41, 451  
 Menten, K. M., Reid, M. J., Forbrich, J., & Brunthaler, A. 2007, *A&A*, 474, 515  
 Minh, Y. C., Ohishi, M., Roh, D. G., Ishiguro, M., & Irvine, W. M. 1993, *ApJ*, 411, 773  
 Müller, H. S. P., Schlöder, F., Stutzki, J., & Winnewisser, G. 2005, *Journal of Molecular Structure*, 742, 215  
 Müller, H. S. P., Thorwirth, S., Roth, D. A., & Winnewisser, G. 2001, *A&A*, 370, L49  
 Neill, J. L., Steber, A. L., Muckle, M. T., et al. 2011, *Journal of Physical Chemistry A*, 115, 6472  
 Neufeld, D. A. & Dalgarno, A. 1989, *ApJ*, 340, 869  
 Nissen, H. D., Cunningham, N. J., Gustafsson, M., et al. 2012, *A&A*, 540, A119  
 Öberg, K. I., Bottinelli, S., Jørgensen, J. K., & van Dishoeck, E. F. 2010, *ApJ*, 716, 825  
 Öberg, K. I., Garrod, R. T., van Dishoeck, E. F., & Linnartz, H. 2009, *A&A*, 504, 891  
 Peeters, Z., Rodgers, S. D., Charnley, S. B., et al. 2006, *A&A*, 445, 197  
 Peng, T. C., Despois, D., Brouillet, N., Parise, B., & Baudry, A. 2012, *A&A*, in press  
 Persson, C. M., Olofsson, A. O. H., Koning, N., et al. 2007, *A&A*, 476, 807  
 Prasad, S. S. & Tarafdar, S. P. 1983, *ApJ*, 267, 603  
 Remijan, A. J., Leigh, D. P., Markwick-Kemper, A. J., & Turner, B. E. 2008, *ArXiv e-prints*  
 Remijan, A. J., Markwick-Kemper, A., & ALMA Working Group on Spectral Line Frequencies. 2007, in *Bulletin of the American Astronomical Society*, Vol. 39, *American Astronomical Society Meeting Abstracts*, 132.11  
 Requena-Torres, M. A., Martín-Pintado, J., Martín, S., & Morris, M. R. 2008, *ApJ*, 672, 352  
 Requena-Torres, M. A., Martín-Pintado, J., Rodríguez-Franco, A., et al. 2006, *A&A*, 455, 971  
 Rodríguez, L. F., Poveda, A., Lizano, S., & Allen, C. 2005, *ApJ*, 627, L65  
 Sandstrom, K. M., Peek, J. E. G., Bower, G. C., Bolatto, A. D., & Plambeck, R. L. 2007, *ApJ*, 667, 1161  
 Schilke, P., Benford, D. J., Hunter, T. R., Lis, D. C., & Phillips, T. G. 2001, *ApJS*, 132, 281  
 Schilke, P., Groesbeck, T. D., Blake, G. A., & Phillips, T. G. 1997, *ApJS*, 108, 301  
 Snyder, L. E., Buhl, D., Schwartz, P. R., et al. 1974, *ApJ*, 191, L79  
 Sutton, E. C., Peng, R., Danchi, W. C., et al. 1995, *ApJS*, 97, 455  
 Turner, B. E. 1989, *ApJS*, 70, 539  
 Turner, B. E. 1991, *ApJS*, 76, 617  
 Zapata, L. A., Schmid-Burgk, J., Ho, P. T. P., Rodríguez, L. F., & Menten, K. M. 2009, *ApJ*, 704, L45  
 Ziurys, L. M. & McGonagle, D. 1993, *ApJS*, 89, 155